JACS
JOURNAL OF THE AMERICAN CHEMICAL SOCIETY
Article
pubs.acs.org/JACS

Ultrafast Dynamics of Photongenerated Holes at a CH_3OH/TiO_2 Rutile Interface

Weibin Chu,[†,‡] Wissam A. Saidi,[§] Qijing Zheng,[*,†,‡] Yu Xie,[⊥,∥] Zhenggang Lan,[⊥,∥] Oleg V. Prezhdo,[¶] Hrvoje Petek,[#] and Jin Zhao[*,†,‡,#]

[†]ICQD/Hefei National Laboratory for Physical Sciences at Microscale, and Key Laboratory of Strongly-Coupled Quantum Matter Physics Chinese, Academy of Sciences and, Department of Physics, and [‡]Synergetic Innovation Center of Quantum Information & Quantum Physics, University of Science and Technology of China, Hefei, Anhui 230026, China

[§]Department of Mechanical Engineering and Materials Science, University of Pittsburgh, Pittsburgh, Pennsylvania 15261, United States

[⊥]Key Laboratory of Biobased Materials, Qingdao Institute of Bioenergy and Bioprocess Technology, Chinese Academy of Sciences, Qingdao, Shandong 266101, China

[∥]University of Chinese Academy of Sciences, Beijing 100049, China

[¶]Departments of Chemistry and Physics and Astronomy, University of Southern California, Los Angeles, California 90089, United States

[#]Department of Physics and Astronomy, University of Pittsburgh, Pittsburgh Pennsylvania 15260, United States

Supporting Information

ABSTRACT: Photogenerated charge carrier dynamics near molecule/TiO_2 interfaces are important for the photocatalytic and photovoltaic processes. To understand this fundamental aspect, we performed a time-domain ab initio nonadiabatic molecular dynamics study of the photogenerated hole dynamics at the CH_3OH/rutile TiO_2(110) interface. We studied the forward and reverse hole transfer between TiO_2 and CH_3OH as well as the hole energy relaxation to the valence band maximum. First, we show that the hole-trapping ability of CH_3OH depends strongly on the adsorption structure. Only when the CH_3OH is deprotonated to form chemisorbed CH_3O will ~15% of the hole be trapped by the molecule. Second, we find that strong fluctuations of the HOMO energies of the adsorbed molecules induced by electron−phonon coupling provide additional channels, which accelerate the hole energy relaxation. Third, we demonstrate that the charge transfer and energy relaxation processes depend significantly on temperature. When the temperature decreases from 100 to 30 K, the forward hole transfer and energy relaxation processes are strongly suppressed because of the reduction of phonon occupation. These results indicate that the molecule/TiO_2 energy level alignment, thermal excitation of a phonon, and electron−phonon coupling are the key factors that determine the photogenerated hole dynamics. Our studies provide valuable insights into the photogenerated charge and energy transfer dynamics at molecule/semiconductor interfaces.

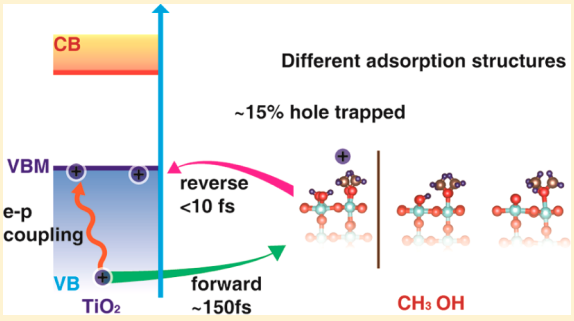

INTRODUCTION

The photocatalytic splitting of H_2O by TiO_2 has become the paradigm for photocatalysis since its seminal discovery by Fujishima and Honda in 1972.[1] Motivated by the prospect of renewable solar energy and environmental remediation, many efforts have been devoted to understanding the fundamental photocatalytic processes as well as to develop new materials and systems based on TiO_2.[2−17] Whereas many studies focus on the net photoconversion efficiency,[2−15,18−20] the understanding at a fundamental level of the various multiple charge transfer steps that occur at the molecular scale at a photocatalytic interface is still lacking.

Photoexcitation of electrons and holes at a photocatalytic interface creates the primary reagents at high potentials, which drive the subsequent redox chemistry. Interfacial charge transfer between semiconductor substrate and molecular media drives photocatalytic reactions in competition with other carrier processes such as energy relaxation, diffusion, trapping, and recombination. Photogenerated charge carriers born in the bulk migrate to the surface, where they can be trapped by the adsorbed molecules and thereby induce catalytic reactions. Both the photogenerated electrons and holes can drive the subsequent chemical reactions. The migration of electrons is typically fast, especially when cocatalysts such as noble metal nanoparticles promote charge separation at the interface.[21−23] By contrast, hole transfer rates are generally slower, and oxidation reactions induced by them require a high over-

Received: August 20, 2016
Published: September 22, 2016

DOI: 10.1021/jacs.6b08725
J. Am. Chem. Soc. 2016, 138, 13740−13749

potential.[21,24] To prevent the recombination of holes with electrons, hole scavengers can be introduced.[25−29]

In photocatalytic studies on TiO_2, methanol has often been employed as an efficient hole scavenger to improve the photocatalytic efficiency.[28,30,31] The electronic structure and photocatalytic activity of CH_3OH chemisorbed on rutile TiO_2(110) surfaces have been studied extensively. Even though the anatase polymorph of TiO_2 has been shown to be more photocatalytically active than rutile, the easy availability and well-developed surface science protocols for the surface preparation have made rutile TiO_2(110) the surface of choice for fundamental studies of photocatalysis. On one hand, many fundamental experimental investigations have addressed the structure and photocatalysis of methanol on TiO_2. Conventional photoemission spectroscopy has been used to measure the electronic structure at the CH_3OH/TiO_2 interface.[32−36] The ultrafast electron dynamics at the molecule/TiO_2 interface have been studied by time-resolved two-photon photoemission (TR-2PP) spectroscopy.[33] Petek, Zhao, and co-workers discovered the "wet electron" acceptor states at 2.4 eV above the Fermi level for H_2O- and CH_3OH-covered TiO_2(110) surfaces.[33,37−39] For the CH_3OH/TiO_2 system, we found that the wet electron state decays by a proton-coupled electron transfer process.[33,38,40] More recently, we investigated how the molecular adsorption affects the t_{2g} to e_g transition among the Ti_{3d} orbitals within the conduction band of TiO_2.[41,42] Other groups have investigated chemistry at the CH_3OH/TiO_2(110) surface. Henderson and co-workers studied the photoinduced reactions of CH_3OH on TiO_2 using temperature-programmed desorption (TPD) techniques; their results suggested that instead of CH_3OH, CH_3O formed by thermal deprotonation is the active species for the hole trapping leading to the formation of CH_2O.[31,43] Such stepwise photoinduced chemical reactions of CH_3OH on TiO_2(110) have also been observed by other groups.[34,35,44−46]

On the other hand, the molecular and electronic structure of the CH_3OH/TiO_2 surface has been investigated at various levels of theory. Previously, we calculated the structure and relative molecular stability, 50% dissociated, and fully dissociated CH_3OH on TiO_2(110), identified various hydrogen-bonding motifs, and found that, in agreement with experiments, the partially dissociated structures are the most stable ones.[47] Migani et al. used methods of many-body perturbation (GW) theory to determine the vertical electron and hole alignment levels for the molecular and dissociated structures.[48,49] Electronic structure calculations both at the density functional theory (DFT) and GW levels implicated CH_3O as the dominant acceptor species on the methanol-covered surfaces. Using nonadiabatic (NA) Ehrenfest dynamics, Kaxiras et al. studied the photon-driven C−H dissociation of CH_3O, which is in agreement with the stepwise photoinduced chemical reactions observed in experiments.[45]

Because CH_3OH is widely known as a hole scavenger, it is very important to understand the dynamics of the photogenerated hole, which initiates the photocatalysis of CH_3OH on TiO_2. As shown schematically in Figure 1, after a photoexcitation, the photogenerated holes start to relax toward the valence band maximum (VBM) of TiO_2 (shown by the blue arrow in Figure 1). During the relaxation, the interface hole may transfer between CH_3OH and TiO_2, as shown by the green arrows in Figure 1. Once the hole is captured by the adsorbate acceptor state, it can energize the reaction or transfer back to the TiO_2 substrate. The relative rates of the forward and reverse charge transfer, as well as the reaction and parasitic processes such as recombination, therefore determine the efficiency of photocatalytic processes. A comprehensive picture of the interface charge transfer dynamics following the hole excitation, however, is still lacking.

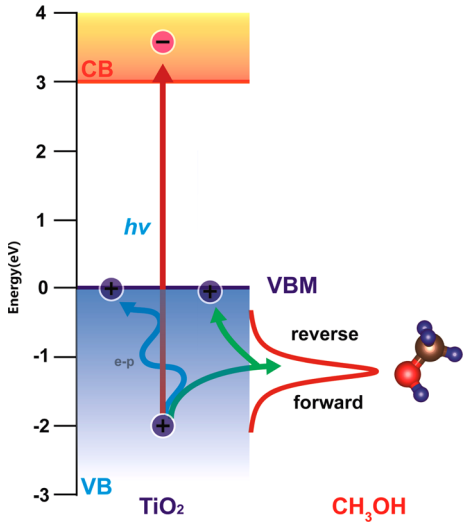

Figure 1. Schematic diagram of photogenerated hole dynamics at the CH_3OH/TiO_2 interface.

In this work, we present a time-domain ab initio study of the hole dynamics at the CH_3OH/TiO_2 interface. Using the nonadiabatic molecular dynamics (NAMD) approach formulated within the framework of time-dependent density functional theory, we obtained valuable insights into the dynamics of photogenerated holes at the CH_3OH/TiO_2 interface. We studied the forward and reverse hole transfer between TiO_2 and CH_3OH as well as the hole relaxation process to VBM. The hole-scavenging ability of CH_3OH is found to strongly depend on the adsorption structure: only the deprotonated CH_3OH in the form of chemisorbed CH_3O is able to trap ∼15% of the hole due to its favorable energy level alignment at the CH_3O/TiO_2 interface. Moreover, the hole energy relaxation to the VBM is strongly affected by the molecular adsorption. The molecular orbitals that are strongly modulated by electron−phonon (e−p) coupling significantly accelerate the relaxation process. Finally, the dynamics of photogenerated holes are found to depend on the temperature. The forward hole transfer from TiO_2 to CH_3OH (hole-trapping process) and the hole relaxation process slow down at lower temperature. The energy level alignment, thermal excitation of phonons, and e−p coupling are the key factors that determine the photogenerated hole dynamics. Our studies provide valuable insights into the photogenerated charge dynamics at the molecule/TiO_2 interface.

METHODOLOGY

Our NAMD study uses DFT as implemented in the Vienna ab initio simulation package to carry out the static and ab initio molecular dynamics calculations.[50−53] The electron−nuclear interactions are described using the projector-augmented wave method.[54] We use the Perdew−Burke−Ernzerhof exchange-correlation functional in all calculations.[55] A 2 × 1 supercell with five layers of TiO_2 describes the CH_3OH/TiO_2 system. The bottom layer Ti and O dangling bonds are saturated with pseudo-hydrogens with nuclear charges of +1.25 and +0.75,

DOI: 10.1021/jacs.6b08725
J. Am. Chem. Soc. 2016, 138, 13740−13749

similar to the protocol of Kowalski and co-workers.[56] A good description for the electronic structure of the system is obtained by sampling the Brillouin zone only at the Γ-point (see Supporting Information, Figure S1). For example, the band gap in our calculation is 1.5 eV, which is in good agreement with 1.7 eV obtained with the primitive unit cell and an 8 × 8 × 1 *k*-point grid.

The time evolution of the excited hole state is obtained using NAMD as implemented within time-dependent DFT developed by Prezhdo's group.[57,58] This method is computationally tractable and has been utilized in several studies of charge transfer and delocalization dynamics in different systems including the wet electrons at the H_2O/TiO_2 interface.[59−62] The electronic structure is calculated using the optimized molecular structure at 0 K. After the geometry optimization, we use velocity rescaling to bring the temperature of the system to either 30 or 100 K; a 5 ps microcanonical ab initio molecular dynamics trajectory is then generated with a time step of 1 fs. Using the molecular dynamics trajectory, the NAMD results are based on averaging over 100 different initial configurations. For each chosen structure, we sample 2×10^4 trajectories for the last 2 ps.[61,63,64] More detailed description of the simulations can be found in the Supporting Information.

RESULTS AND DISCUSSION

Geometry and Electronic Structure of the CH_3OH/TiO_2 Interface. In our study, we consider one-monolayer (ML) structures defined by 100% occupation of five coordinated Ti (Ti_{5C}) sites, where CH_3OH molecules form a bond through their O atoms. We investigate the (2 × 1) surface cell, where two methanol molecules correspond to the full occupation. The two molecules can exist in three different adsorption structures and are indicated as M (molecular), HD (half-dissociated), and D (fully dissociated), as shown in Figure 2. Methanol molecules

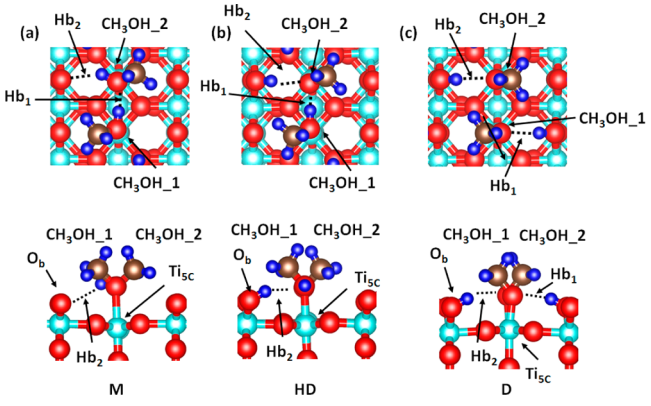

Figure 2. Top and side views of the most stable molecular (M), half-dissociated (HD), and fully dissociated (D) adsorption structures. CH_3OH_1 and CH_3OH_2 label different methanol molecules in the unit cell, and Hb_1 and Hb_2 are their hydrogen bonds. The cyan, red, brown, and blue balls represent Ti, O, C, and H atoms, respectively.

can adopt intermolecular or molecule−surface hydrogen-bonding motifs. Although there are other structures with different patterns of hydrogen bonds, the selected structures are the most stable ones according to a previous DFT calculation.[47] The calculated adsorption energies (E_{ads}) per molecule and molecule−surface Ti−O (Ti−O_m) bond lengths of these structures are listed in Table 1. In the rest of the paper, we label the two adsorbed molecules in the supercell as CH_3OH_1 and CH_3OH_2, respectively. In the M case, one CH_3OH (CH_3OH_1) forms a hydrogen bond (Hb) to a bridging oxygen (O_b) atom (Hb_1) of the substrate, while the other molecule (CH_3OH_2) binds less strongly with the surface and forms an intermolecular Hb_2 with the first molecule. The HD structure is obtained from the M structure by transferring H^+ to the proximate surface O_b atom such that now the Hb_1 consists of surface OH interacting with the O atom of the CH_3O. In the D structure, both methanol molecules are fully deprotonated, transferring their H^+ to the adjacent O_b sites. The deprotonation of the CH_3OH strengthens the Ti−O_m bond. From Table 1, one can see that the interface Ti−O_m bond lengths decrease by 0.5 Å from the M to D structures.

Table 1. Average Adsorption Energies, Bond Lengths of Hbs and Ti−O_m Bonds and Averaged Energies of the Molecular HOMO Levels Relative to the VBM for M, HD, and D Structures

	E_{ads} (eV)	Hb_1 (Å)	Hb_2 (Å)	Ti−O_m (Å) (CH_3OH_1)	Ti−O_m (Å) (CH_3OH_2)	E_{HOMO} (eV)
M	0.553	1.68	2.55	2.37	2.42	−1.59
HD	0.644	1.53	2.17	2.22	1.98	−0.71
D	0.535	2.14	2.24	1.87	1.86	−0.26

Before presenting the NAMD calculations, it is instructive to establish the energetics of the localized hole states of the three adsorption structures based on the calculated valence band (VB) electronic structures. Figure 3a shows the total and partial

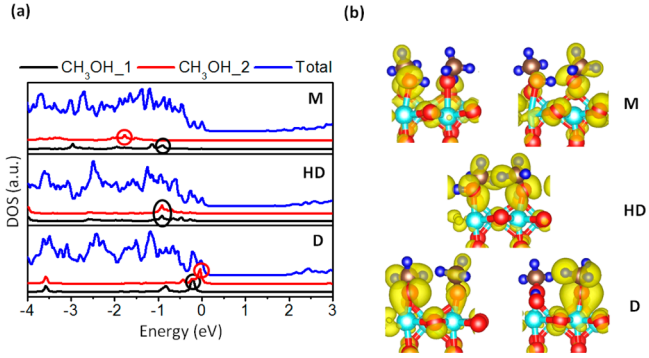

Figure 3. (a) Total (blue) and partial (black and red) DOS contributed by adsorbed molecules for M, HD, and D structures. The reference energy is VBM. (b) Spatial orbital distributions of HOMOs of adsorbed molecules.

density of states (DOS) contributed by CH_3OH_1 and CH_3OH_2. The VBM is set to be the energy reference. The highest energy peak in the partial DOS contributed by adsorbed molecules corresponds to the highest occupied molecular orbitals (HOMOs) substantially localized on methanol or methoxy, which are shown in Figure 3b. As seen from the figure, these molecular orbitals are strongly hybridized with the orbitals of the TiO_2 substrate. By performing a partial DOS analysis, we find that HOMOs of the M, HD, and D structures have around 85, 70 and 55% charge probability distributed on the TiO_2 substrate as an average of two adsorbed molecules within the unit cell. If we compare in detail the partial DOS contributed by the adsorbates in these three structures, it is evident that the DOS of methoxy is closer to the VBM, and its charge density is more localized on the molecule than for methanol. These results are in good agreement with previous

DOI: 10.1021/jacs.6b08725
J. Am. Chem. Soc. 2016, 138, 13740−13749

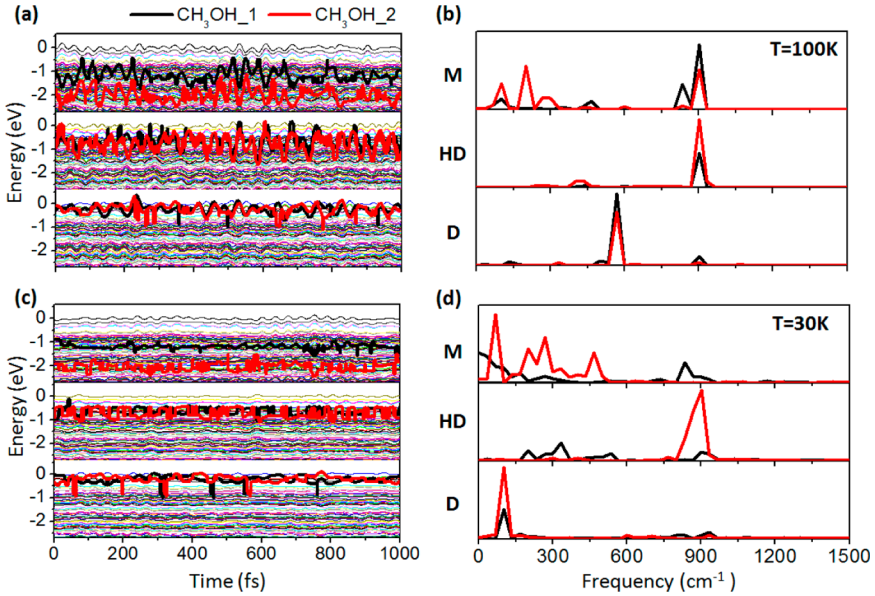

Figure 4. Time-dependent evolution of the molecular HOMO energy of adsorbed molecules for the M, HD, and D structures (a,c) and their Fourier transform spectra (b,d) at 100 and 30 K. The reference energy is the averaged VBM. The thick black and red lines represent the molecular HOMO of CH_3OH_1 and CH_3OH_2, and the thin lines in (a,c) show other energy states of TiO_2.

investigations using DFT as well as the high-level GW quasi-particle calculations.[47,65,66]

Thermal Fluctuation of the Hole-Trapping State. Because methanol is known as a hole scavenger, we anticipate that the HOMOs of methanol and methoxy on TiO_2 act as the molecular hole-trapping states at the interface. In Figure 4a, we plot the energy evolution of these hole-trapping states during a 1 ps MD run at 100 K. The HOMOs are identified by choosing the state which has the biggest contribution from the adsorbed molecules above −2.5 eV. During an MD trajectory, e−p coupling occurs by adiabatic (AD) processes, where the thermally excited nuclear motions drive fluctuations of the hole state's energy, and NA processes, where the nuclear velocities modulate the electronic coupling matrix elements. The fluctuation amplitudes reflect the strength of the e−p coupling. For all three structures, the energy fluctuations of molecular hole-trapping states are as large as 1.3−1.5 eV. By contrast, the range of fluctuation of TiO_2 VB states near VBM is smaller than 0.5 eV. The much larger fluctuations of the molecular states signify that they experience much stronger e−p coupling. Thus, the large swings of the HOMO energies cause many crossings with the VB states of the substrate during a 1 ps MD trajectory. The averaged HOMO energy over CH_3OH_1 and CH_3OH_2 and over MD trajectory at 100 K (E_{HOMO}) is shown in Table 1. In agreement with the static limit of the orbitals shown in Figure 3, the HOMO of methoxy is closer to VBM. In structure D, during the 1 ps MD trajectory, 12% of HOMOs of methoxy contribute to the VBM of the whole system.

Specific vibrational modes modulate the hole state energies. The dominant modes contributing to e−p coupling can be identified from the Fourier transform (FT) spectra of the energy trajectories of the molecular HOMOs for the different adsorption structures, as shown in Figure 4b. The FT spectra can be interpreted by analyzing the vibrational modes of the system based on DFT calculations. For example, for the M structure, the peaks around 150 cm^{-1} are associated with the Hb vibrations; the peaks around 300 and 500 cm^{-1} are associated with the $Ti-O_m$ stretching mode and the TiO_2 surface-localized vibrations; and the peaks around 900 cm^{-1} are associated with the C−O stretching mode of CH_3OH. Because CH_3OH is adsorbed on TiO_2 by forming a $Ti-O_m$ bond, the C−O and $Ti-O_m$ stretching modes are coupled. This spectral fingerprint is similar for the HD structure except that $Ti-O_m$ stretching for the CH_3O species has a component at 400 cm^{-1}. For the fully dissociated D structure, the main peaks are around 600 cm^{-1}, which correspond to the $Ti-O_m$ vibration, while the remaining weaker 900 cm^{-1} peaks correspond to the C−O stretching mode. Therefore, for all three structures, the thermal fluctuation of molecular HOMOs is mainly driven by the $Ti-O_m$ and C−O stretching modes. This can be understood by checking the HOMO distribution shown in Figure 3b, in which one can see that the π^* orbital between C and O has a significant contribution. Besides that, there is also hybridization between O_{2p} with Ti_{3d}. For the D structure, the deprotonation induces stronger interaction between TiO_2 and CH_3O, as can be seen from the change of $Ti-O_m$ bond length from 2.37 and 2.42 Å to 1.86 and 1.87 Å. The hybridization becomes stronger, and therefore, the major contribution for the D structure is from the $Ti-O_m$ stretching. The high-frequency O_bH stretching mode, which has been found to modulate the wet electron states,[61] appears to be silent in modulation of the hole acceptor states at 100 K.

Dynamics of a Photogenerated Hole. Figure 1 shows schematically the photon-generated hole dynamics processes that influence the efficiency of photocatalysis. After the excitation, the photogenerated holes undergo energy relaxation to the VBM. During this process, there might be interfacial hole transfer between TiO_2 and the molecule. Therefore, in the following, we discuss the competition between hole transfer and energy relaxation at 100 K.

Forward Hole Transfer from TiO_2 to Adsorbates. The forward hole transfer from TiO_2 to adsorbates, where TiO_2 bulk bands act as the donor states and HOMOs of adsorbates are the acceptor states, as shown in Figure 1, determines the hole-scavenging properties of adsorbed molecules. To study

DOI: 10.1021/jacs.6b08725
J. Am. Chem. Soc. 2016, 138, 13740−13749

this process, we initiated the NAMD calculations with a hole mostly localized in TiO_2 at a specific energy. We considered three such states with initial hole energies $[E_h(0)]$ at approximately −0.4, −0.6, and −1.0 eV below the E_{HOMO}. As shown in Figure 5a, the forward hole transfer for the M, HD, and D structures shows significantly different behavior. At t = 0 fs, the hole localization on TiO_2 is higher than 90% for all three structures. For the M structure, there is almost no forward hole transfer from TiO_2 to the molecule; the hole localization in the TiO_2 region remains higher than 95%, unaltered by the thermal fluctuations. By contrast, for the D structure, around 20% hole transfers to the molecule on an average time scale of 150 fs. Around 300 fs, the hole localization on TiO_2 decreases to 80%. After that, there is some charge oscillation indicating that both forward and reverse charge transfers happen between TiO_2 and the molecule, but the total hole localization on TiO_2 remains at around 85%. The forward hole transfer from different initial energy states shows no significant difference after 300 fs.

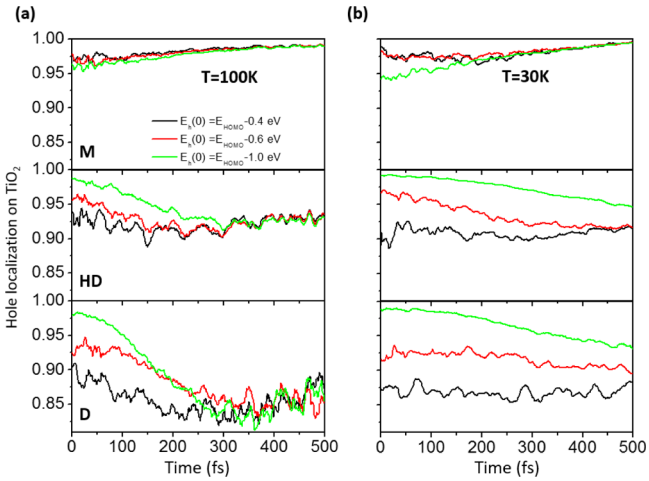

Figure 5. Averaged forward hole transfer from TiO_2 bulk states to adsorbed molecules at (a) 100 and (b) 30 K.

Because of the strong hybridization between the orbitals of TiO_2 and adsorbed methanol, there is significant orbital delocalization in TiO_2 for the acceptor HOMOs of adsorbed molecules. This implies that even if the holes are completely transferred to the HOMOs of adsorbate, there will still be a large component of the hole density delocalized in TiO_2. To make this forward hole transfer process more meaningful, we analyzed the statistics of the time-dependent proportion of hole transfer from TiO_2 to the HOMO of adsorbate for M, HD, and D structures by averaging the forward hole transfer from different initial energy donor states, as shown in Figure 6a. One can see that for the M structure, the proportion of hole transfer to HOMO increases to around 10% within the first 100 fs and then decreases to almost zero at 500 fs. By contrast, for the HD and D structures, it increases to 30 and 45% within the first 300 fs and then generally decreases to 25 and 30% at 500 fs.

During a molecular dynamics trajectory, both the AD and NA mechanisms contribute to the charge transfer. AD charge transfer is provoked by nuclear motion, which causes the energy states to cross, thereby promoting charge transfer. Charge transfer can also occur by the NA process through direct charge hopping between different states with a different amount of hole density on the molecular overlayer. These two mechanisms can be distinguished in the time propagation

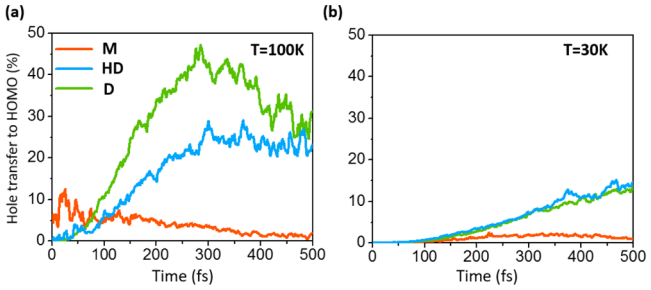

Figure 6. Averaged proportion of forward hole transfer to molecular HOMO at (a) 100 and (b) 30 K.

equations of motion,[61] as described in the Supporting Information. In Figure 7a, we show separately the NA and AD contributions to the forward hole transfer process at 100 K. For the M structure, both the NA and AD components are very small, which is not surprising because the hole remains largely on TiO_2. By contrast, for the HD and D structures, the NA and AD mechanisms have the opposite contributions to the hole transfer. The NA mechanism favors the probability of hole hopping to the molecular HOMO because it is energetically favored. The AD mechanism promotes the reverse hole transfer from molecules to the TiO_2 surface because it is possible for the hole to transfer back to TiO_2 by the AD mechanism whenever the HOMO crosses the TiO_2 states, and the strong HOMO energy oscillation shown in Figure 4a favors such transfer. Overall, the NA mechanism is dominant because it is energetically favored, causing the partial hole transfer from TiO_2 to adsorbed molecules.

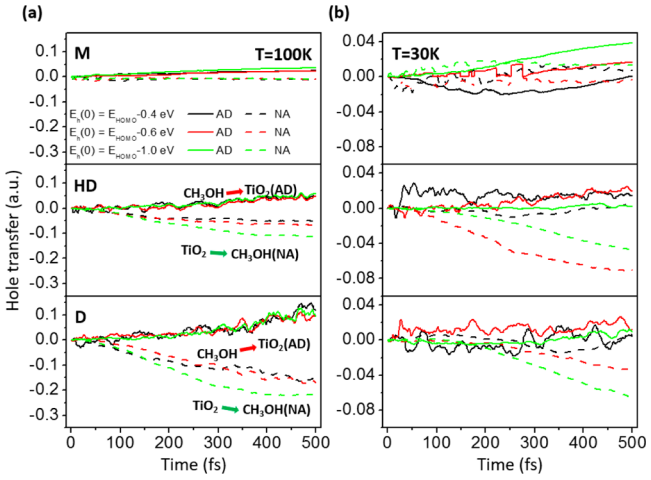

Figure 7. NA and AD contributions to the forward hole transfer from TiO_2 to adsorbed molecules for the M, HD, and D structures at (a) 100 K and (b) 30 K.

Reverse Hole Transfer from Adsorbates to TiO_2. The reverse hole transfer from adsorbates to TiO_2 determines the lifetime of trapped holes, and therefore, it also affects the efficiency of photocatalysis. To study these processes, we perform the NAMD calculations with a hole initially localized on HOMOs of CH_3OH_1 or CH_3OH_2 that are shown in Figure 3b.

As already noted, the orbital hybridization between CH_3OH with TiO_2 already has substantial initial hole density within the TiO_2 surface. Thus, only a fraction of the hole remains to be transferred from the molecules to the surface. The NAMD

DOI: 10.1021/jacs.6b08725
J. Am. Chem. Soc. 2016, 138, 13740−13749

simulations indeed find the reverse hole transfer to be ultrafast. For all different adsorption structures, the reverse hole transfer happens within 10 fs, as shown in Figure 8a. The only

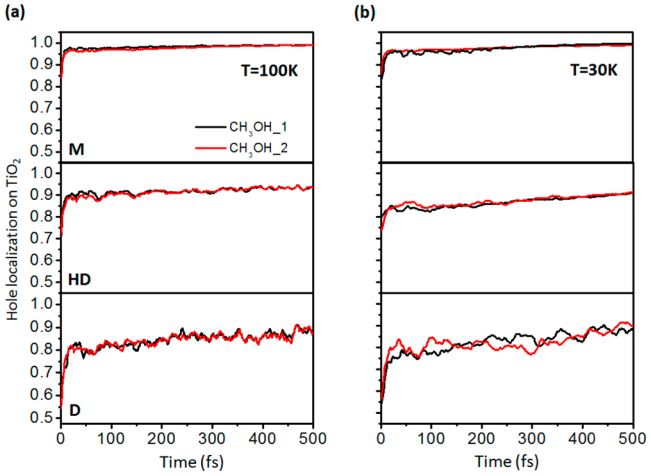

Figure 8. Averaged hole reverse transfer from adsorbed molecules to TiO_2 bulk states at (a) 100 K and (b) 30 K.

surprising result is that for the D structure, which has the highest percentage of molecule-localized hole density (45% hole on CH_3O), after the initial back hole transfer process, around 20% of the hole remains on the CH_3O, which can still promote photocatalysis. By contrast, the hole transfer into the TiO_2 for the M structure is nearly complete. These results are qualitatively in agreement with the forward hole transfer dynamics. Another significant difference between different adsorption structures is that, for the HD and especially the D structure, there is a charge oscillation after the reverse hole transfer that is not observed for the M structure, as seen in Figure 8a. In the forward hole transfer process, we observe similar oscillation as already described. This oscillation is due to the large hole density on the D structure and the relatively small DOS of the substrate, such that there is a significant chance for the hole density to oscillate between them.

The ultrafast reverse hole transfer time scale of around 10 fs is mainly determined by the AD mechanism, as shown in Figure 9a. This is because there is a high DOS contributed by TiO_2 at

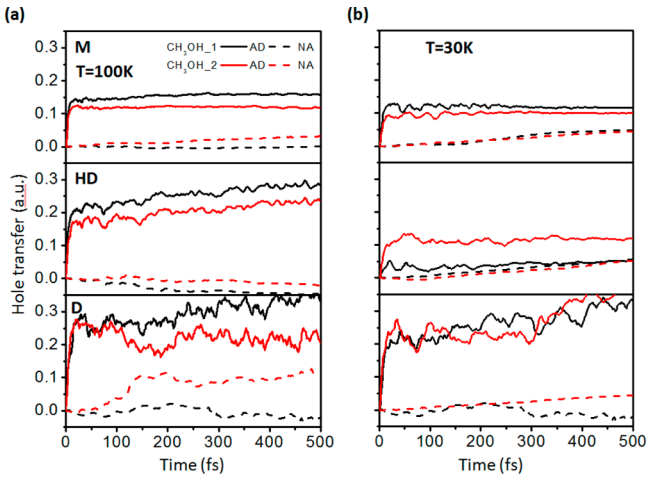

Figure 9. AD and NA contribution of reverse hole transfer from adsorbed molecules to TiO_2 at (a) 100 K and (b) 30 K.

the energy of the HOMO of adsorbed molecules (Figure 3). The HOMO state crosses many of the TiO_2 VB states during an MD run, as shown in Figure 4a. This multitude of crossings can lead to efficient AD charge transfer. Simply, the initially localized electronic wave packet dephases into bulk states of TiO_2 through the thermal nuclear motion. Here, the fact that all of the M, HD, and D structures do not show significant differences suggests that the C−O stretching mode at 900 cm^{-1} plays an important role in the reverse hole transfer. The ultrafast time scale of 10 fs is approximately one-quarter cycle of the C−O stretching mode with the period of 37 fs.

Hole Energy Relaxation to VBM. Besides the forward and reverse hole transfers between molecule and TiO_2, we also investigated the rates of the energy relaxation to VBM through e−p coupling. The hole is initially created with a specific energy $E_h(0)$. During the relaxation, however, the average hole energy $E_h(t)$ is time-dependent. We computed $E_h(t)$ as a function of time for a range of initial hole excitation energies where, again, the average energy of VBM is the reference. We chose the initial hole energies $E_h(0)$ to be −2.0, −1.5, and −1.0 eV within bands of the bulk TiO_2.

Figure 10a shows the time-dependent hole energy relaxation to VBM at 100 K. The calculations are performed for the three

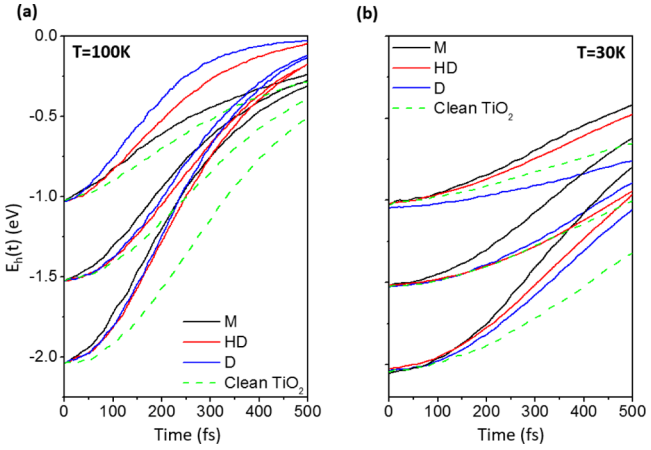

Figure 10. Time dependence of energy relaxation of the photogenerated holes with different initial energies at (a) 100 K and (b) 30 K.

adsorption structures, as well as the clean TiO_2 surface. We found that molecular adsorption accelerates the hole energy relaxation to VBM. This adsorption-induced acceleration is significant for the three adsorption structures when the initial hole state energy is $E_h(0) = -2.0$ eV. By contrast, when $E_h(0) = -1.0$ eV, the acceleration is still distinct for the D structure; however, for the M structure, the relaxation process is quite similar to that of the clean TiO_2 surface. We attribute this adsorption-induced acceleration to the relatively strong e−p coupling of the HOMOs of the adsorbed molecules; the molecular adsorption causes the strong time-dependent energy fluctuations that are already introduced in Figure 2a. The fluctuations cause level crossings and thus charge transfer, which contributes additional charge energy relaxation channels. Naturally, such acceleration depends on the energy range distribution of the HOMOs. From Figure 2a, one can see that the HOMOs are located within the range from −2.5 to −0.8 eV for the M structure and thus they only accelerate the hole relaxation within this energy range. Therefore, for $E_h(0) = -1.0$

DOI: 10.1021/jacs.6b08725
J. Am. Chem. Soc. 2016, 138, 13740−13749

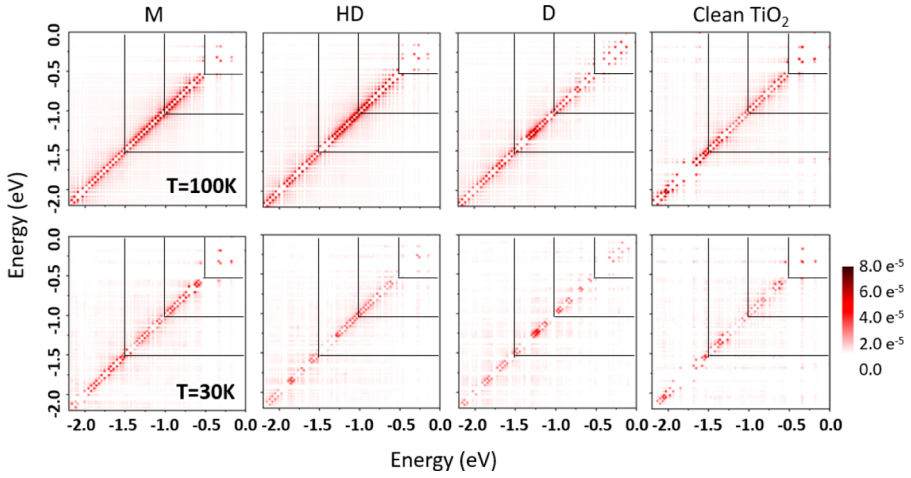

Figure 11. Distribution of averaged NA coupling along 2 ps NAMD trajectory between electronic states at different energies. The averaged VBM is set to be the energy reference.

eV, the acceleration of hole relaxation for the M structure is not distinct. For the D structure, the hole relaxation acceleration is significant for $E_h(0) = -1.0$ eV because its HOMOs are located within the energy range from −1.1 to 0 eV.

Temperature Dependence. Our results show that both the hole transfer and relaxation processes are promoted by phonon excitation and thus should be temperature-dependent. To verify this, we performed the NAMD calculations at a lower temperature of 30 K, which is expected to reduce the phonon occupation and therefore the oscillation amplitude with respect to 100 K. The results are also shown in panels c and d in Figure 4 and panel b in Figures 5−10. From Figures 5−7, one can see that cooling the sample to 30 K strongly suppresses the forward hole transfer. Figure 7b shows that this suppression happens both for the NA and AD components. Figures 8 and 9 show that the reverse hole transfer at 30 K retains the ultrafast character because the C−O stretching mode at 900 cm^{-1} is not completely frozen, as shown in Figure 4d, and the high DOS around the HOMOs makes the reverse hole transfer very efficient. Figure 10 clearly shows that hole energy relaxation to VBM is decelerated at 30 K.

The suppression of AD charge transfer is easy to understand because it is provoked by nuclear motion and thus strongly coupled to the phonon excitation. The NA charge transfer is determined by the NA coupling matrix, where the interaction between the electronic states j and k can be expressed in terms of their energy difference as

$$d_{jk} = \langle j|\nabla_R|k\rangle \cdot \dot{R} = \frac{\langle j|\nabla_R \hat{H}|k\rangle}{\varepsilon_k - \varepsilon_j}\dot{R} \quad (1)$$

In eq 1, H is the Kohn−Sham Hamiltonian, ε_k is the eigenvalue for electronic state k, and $\dot{R}$ is the time derivative of the nuclei positions.[67] Thus, NA couplings show strong dependence on the energy difference of the interacting states, the orbital distribution of states k and j, and the nuclear velocity. The nuclear velocity is determined by the frequency and amplitude of vibration and is thus related to e−p coupling and phonon excitation and, therefore, is also temperature-dependent. In Figure 11, we plot the averaged NA couplings between different states along the 2 ps NAMD trajectory for the M, HD, and D adsorption structures and the clean TiO_2 surface at 100 and 30 K. It is clear that the NA couplings decrease with the temperature. At 30 K, when the phonon occupation is distinctly decreased, the hole relaxation strongly depends on the NA couplings. For example, from Figure 10b, one can see that the hole relaxation for the D structure is the slowest within the energy range of [−1.0 eV, −0.5 eV]. This is because the NA couplings for the D structure in this energy range are the weakest. In contrast, within the energy range of [−0.5 eV, 0.0 eV], the NA coupling for the D structure is the strongest. That explains why the forward NA hole transfer in the D structure is the most significant, as shown in Figure 7.

DISCUSSION

Our results show that molecular adsorption plays an important role in the dynamics of interfacial hole transfer and hole relaxation at the rutile molecule/TiO_2(110) interface. The crucial factors influencing the dynamics include (i) energy level alignment between TiO_2 and adsorbed molecules; (ii) e−p coupling and phonon excitation of molecular states; and (iii) NA couplings between electronic states. First, the energy level alignment determines the hole-trapping ability. All of our results suggest that CH_3O and not CH_3OH is the possible hole-trapping site on TiO_2. From Figure 3b, one can find a significant hole distribution on the C atom, which may play a role in the hole-mediated deprotonation of CH_3O. This is in agreement with the picture given by different experiments where the deprotonation of CH_3OH is thermally assisted but the subsequent deprotonation of CH_3O is hole-mediated.[34,43−46] The main reason why CH_3O is the dominant trapping site is that its HOMO is very close to the VBM of TiO_2. We would expect that this molecule/TiO_2 energy level alignment is sensitive to different TiO_2 surfaces and other environmental factors. For example, Sun et al. have shown that HOMO of CH_3OH on an anatase TiO_2(101) surface is closer to the VBM compared with rutile TiO_2(110).[68] Ji et al. have shown that on the anatase TiO_2(101) surface, molecular CH_3OH has the HOMO very close to the VBM, whereas for the dissociated CH_3O, it is even above the VBM.[69] Such energy level alignments are fully consistent with the relative photochemical activity of CH_3OH versus CH_3O adsorbates as well as the rutile versus anatase substrates. Cheng et al. reported that thermal fluctuations and solvent environment play an important role in energy level alignment at the H_2O/anatase TiO_2(101) surface.[70] Thus, the HOMO energy level alignment

DOI: 10.1021/jacs.6b08725
J. Am. Chem. Soc. 2016, 138, 13740−13749

relative to the VBM of TiO_2 is the crucial aspect for the photocatalytic activity.

Second, the time scales for the interfacial hole transfer and relaxation are strongly affected by the thermal excitation of the nuclear motion (e.g., phonon excitation) and the e−p coupling. In the case of the AD charge transfer, the fluctuation of molecular states induced by e−p coupling brings the interacting levels into resonance, thereby promoting charge and energy transfer. In the case of NA charge transfer, the NA matrix elements are affected by phonon excitation and e−p coupling through the nuclear velocities. At 100 K, the NA and AD mechanisms compete in promoting the forward hole transfer from TiO_2 to CH_3OH on a time scale of 150 fs. The reverse hole transfer from CH_3OH to TiO_2 is assisted by the C−O stretching mode at 900 cm^{-1} and happens within 10 fs. For the hole energy relaxation process, the strong fluctuations of the HOMOs induced by e−p coupling of the adsorbed molecules provide additional hole relaxation channels and accelerate the hole relaxation processes. The thermal excitation of the nuclear motion and e−p coupling are sensitive to the TiO_2−molecule interaction and thus can vary for different adsorption structures, coverages, surfaces, and environmental factors such as solvent environment. Batista and Rego et al. have studied the influence of thermal fluctuation on electron injection at dye/TiO_2 interface since 2005.[71−73] In their early work, they found that thermal nuclear fluctuations speed up the underlying interfacial electron transfer dynamics by introducing nonadiabatic transitions between electron acceptor states, localized in the vicinity of the photoexcited adsorbate, and delocalized states extended throughout the semiconductor material, creating additional relaxation pathways for carrier diffusion.[71] Their recent results show that the electron transfer at the dye/TiO_2 interface is driven by a strong coupling between electron dynamics and specific nuclear vibrational modes.[73] Methanol has strongly crystal-face- and polymorph-dependent adsorption structures, and thus similar studies of the hole dynamics for related systems should achieve a better understanding of the photocatalytic properties of TiO_2.

Furthermore, because thermal excitation of nuclear motion is important, the dynamics of photogenerated hole shows strong temperature dependence. The forward hole transfer process and the hole relaxation process can be strongly suppressed at 30 K because of the decrease of the phonon occupation and NA coupling. Our results thus suggest that temperature might be a significant factor in controlling the photocatalytic properties of TiO_2 surfaces.

Hole transfer and the relaxation process at TiO_2 surfaces have been studied by two other approaches. Kolesov et al. investigated the light-driven dissociation process of CH_3O using Ehrenfest dynamics.[45] Their work clearly reveals the reaction intermediates, time scales, and energetics. In contrast to their approach, the NAMD calculations reported here are based on the fewest switches surface hopping method, applying the classical path approximation,[58] which is based on the assumption that the nuclear dynamics of the system remain unaffected by the dynamics of the electronic degrees of freedom. Therefore, in our approach, such a kind of photochemical process cannot be simulated. We provide, however, a comprehensive study of the hole dynamics including the forward and reverse hole transfer, as well as the hole energy relaxation. The important role of energy level alignment and e−p coupling is revealed. The other study was performed by Zhukov et al., who investigated the hole−phonon relaxation process at the TiO_2 surface.[74] They calculated the quasi-stationary distribution function of the photogenerated hole based on the "Fermi golden rule" of perturbation theory. They obtained a time scale of 40 fs of hole energy relaxation from −2.0 eV to VBM, which is faster than our results. As discussed by Zhukov et al., an experimental measurement done by Morishita et al. using the femtosecond transient reflecting grating technique gave hole relaxation times of no less than 110 to 690 fs,[75] which is in better agreement with our results. Yet the use of the classical path approximation and lack of accounting for electron−electron interactions in our calculations likely underestimates hole relaxation rates in our calculations. Further progress in understanding the hole dynamics in TiO_2 can be obtained by directly measuring the hole distribution functions by methods such as time-resolved photoemission.[76]

CONCLUSIONS

Using an ab initio NAMD approach, we studied the dynamics of photogenerated holes at a CH_3OH/TiO_2 interface for different adsorption structures. We have investigated the forward and reverse hole transfer between TiO_2 and CH_3OH as well as the hole energy relaxation to VBM. First, we found that the hole-trapping ability of CH_3OH strongly depends on the adsorption structure. Only when the CH_3OH is deprotonated to form chemisorbed CH_3O will there be ∼15% hole trapped by the molecule at 100 K. Second, we found that the strong fluctuations of the HOMO energies induced by the e−p coupling provide an additional hole relaxation channel that accelerates the hole relaxation process. Third, we found the dynamics of photogenerated holes to be strongly temperature dependent. When the temperature is decreased from 100 to 30 K, the hole forward transfer and hole relaxation processes are strongly suppressed because of the reduction of the phonon occupations. These results suggest that the energy level alignment, phonon excitation, and e−p couplings are the three key factors that determine the photogenerated hole dynamics in TiO_2 and other photocatalytic systems. The specific interactions of CH_3OH and CH_3O with TiO_2(110) surfaces show that the thermal chemisorption chemistry also plays an important role in photocatalysis. Our results are general and can be extended to other photocatalytic systems.

ASSOCIATED CONTENT

Supporting Information

The Supporting Information is available free of charge on the ACS Publications website at DOI: 10.1021/jacs.6b08725.

Additional details and figures (PDF)

AUTHOR INFORMATION

Corresponding Authors

*zqj@mail.ustc.edu.cn

*zhaojin@ustc.edu.cn

Notes

The authors declare no competing financial interest.

ACKNOWLEDGMENTS

J.Z. acknowledges the support of Natural Science Foundation of Science of China (Grant Nos. 11322434, 21121003, and 11620101003) and Chinese Department of Science & Technology (Grant Nos. 2016YFA0200600 and

2016YFA0200604). H.P. and J.Z. acknowledge the support of National Science Foundation (Grant Nos. CHE-1213189 and CHE-1565704). Z.L. acknowledges the support of Natural Science Foundation of Science of China (Grant Nos. 21503248, 21543008, and 21673266) and Natural Science Foundation of Shandong Province for Distinguished Young Scholars (JQ201504). O.V.P. acknowledges support of the U.S. Department of Energy (Grant No. DE-SC0014429). Calculations were performed at the Environmental Molecular Sciences Laboratory at the PNNL, a user facility sponsored by the DOE Office of Biological and Environmental Research.

REFERENCES

(1) Fujishima, A.; Honda, K. *Nature* **1972**, *238*, 37.
(2) Li, H. X.; Bian, Z. F.; Zhu, J.; Zhang, D. Q.; Li, G. S.; Huo, Y. N.; Li, H.; Lu, Y. F. *J. Am. Chem. Soc.* **2007**, *129*, 8406.
(3) Han, X. G.; Kuang, Q.; Jin, M. S.; Xie, Z. X.; Zheng, L. S. *J. Am. Chem. Soc.* **2009**, *131*, 3152.
(4) Xiang, Q. J.; Yu, J. G.; Jaroniec, M. *J. Am. Chem. Soc.* **2012**, *134*, 6575.
(5) Yang, H. G.; Liu, G.; Qiao, S. Z.; Sun, C. H.; Jin, Y. G.; Smith, S. C.; Zou, J.; Cheng, H. M.; Lu, G. Q. *J. Am. Chem. Soc.* **2009**, *131*, 4078.
(6) Liu, S. W.; Yu, J. G.; Jaroniec, M. *J. Am. Chem. Soc.* **2010**, *132*, 11914.
(7) Livraghi, S.; Paganini, M. C.; Giamello, E.; Selloni, A.; Di Valentin, C.; Pacchioni, G. *J. Am. Chem. Soc.* **2006**, *128*, 15666.
(8) Wang, J.; Tafen, D. N.; Lewis, J. P.; Hong, Z. L.; Manivannan, A.; Zhi, M. J.; Li, M.; Wu, N. Q. *J. Am. Chem. Soc.* **2009**, *131*, 12290.
(9) Chen, X. B.; Burda, C. *J. Am. Chem. Soc.* **2008**, *130*, 5018.
(10) Santra, P. K.; Kamat, P. V. *J. Am. Chem. Soc.* **2012**, *134*, 2508.
(11) Youngblood, W. J.; Lee, S. H. A.; Kobayashi, Y.; Hernandez-Pagan, E. A.; Hoertz, P. G.; Moore, T. A.; Moore, A. L.; Gust, D.; Mallouk, T. E. *J. Am. Chem. Soc.* **2009**, *131*, 926.
(12) Zuo, F.; Wang, L.; Wu, T.; Zhang, Z. Y.; Borchardt, D.; Feng, P. Y. *J. Am. Chem. Soc.* **2010**, *132*, 11856.
(13) Naldoni, A.; Allieta, M.; Santangelo, S.; Marelli, M.; Fabbri, F.; Cappelli, S.; Bianchi, C. L.; Psaro, R.; Dal Santo, V. *J. Am. Chem. Soc.* **2012**, *134*, 7600.
(14) Ingram, D. B.; Linic, S. *J. Am. Chem. Soc.* **2011**, *133*, 5202.
(15) Yu, J. G.; Low, J. X.; Xiao, W.; Zhou, P.; Jaroniec, M. *J. Am. Chem. Soc.* **2014**, *136*, 8839.
(16) Feng, X. J.; Zhu, K.; Frank, A. J.; Grimes, C. A.; Mallouk, T. E. *Angew. Chem., Int. Ed.* **2012**, *51*, 2727.
(17) Swierk, J. R.; Mallouk, T. E. *Chem. Soc. Rev.* **2013**, *42*, 2357.
(18) Zhu, W. G.; Qiu, X. F.; Iancu, V.; Chen, X. Q.; Pan, H.; Wang, W.; Dimitrijevic, N. M.; Rajh, T.; Meyer, H. M.; Paranthaman, M. P.; Stocks, G. M.; Weitering, H. H.; Gu, B. H.; Eres, G.; Zhang, Z. Y. *Phys. Rev. Lett.* **2009**, *103*, 226401.
(19) Gai, Y.; Li, J.; Li, S.-S.; Xia, J.-b.; Wei, S.-H. *Phys. Rev. Lett.* **2009**, *102*, 036402.
(20) Li, X.; Li, Z.; Yang, J. *Phys. Rev. Lett.* **2014**, *112*, 018301.
(21) Simon, T.; Bouchonville, N.; Berr, M. J.; Vaneski, A.; Adrovic, A.; Volbers, D.; Wyrwich, R.; Doblinger, M.; Susha, A. S.; Rogach, A. L.; Jackel, F.; Stolarczyk, J. K.; Feldmann, J. *Nat. Mater.* **2014**, *13*, 1013.
(22) Kamat, P. V. *J. Phys. Chem. Lett.* **2012**, *3*, 663.
(23) Mongin, D.; Shaviv, E.; Maioli, P.; Crut, A.; Banin, U.; Del Fatti, N.; Vallee, F. *ACS Nano* **2012**, *6*, 7034.
(24) Nozik, A. J. *Nature* **1975**, *257*, 383.
(25) Sakai, N.; Fujishima, A.; Watanabe, T.; Hashimoto, K. *J. Phys. Chem. B* **2003**, *107*, 1028.
(26) Nakamura, R.; Nakato, Y. *J. Am. Chem. Soc.* **2004**, *126*, 1290.
(27) Shkrob, I. A.; Sauer, M. C. *J. Phys. Chem. B* **2004**, *108*, 12497.
(28) Thompson, T. L.; Yates, J. T. *J. Phys. Chem. B* **2005**, *109*, 18230.
(29) Kawai, T.; Sakata, T. *J. Chem. Soc., Chem. Commun.* **1980**, 694.
(30) Tamaki, Y.; Furube, A.; Murai, M.; Hara, K.; Katoh, R.; Tachiya, M. *J. Am. Chem. Soc.* **2006**, *128*, 416.
(31) Henderson, M. A. *Surf. Sci. Rep.* **2011**, *66*, 185.
(32) Onishi, H.; Aruga, T.; Egawa, C.; Iwasawa, Y. *Surf. Sci.* **1988**, *193*, 33.
(33) Li, B.; Zhao, J.; Onda, K.; Jordan, K. D.; Yang, J.; Petek, H. *Science* **2006**, *311*, 1436.
(34) Yuan, Q.; Wu, Z.; Jin, Y.; Xu, L.; Xiong, F.; Ma, Y.; Huang, W. *J. Am. Chem. Soc.* **2013**, *135*, 5212.
(35) Zhou, C. Y.; Ren, Z. F.; Tan, S. J.; Ma, Z. B.; Mao, X. C.; Dai, D. X.; Fan, H. J.; Yang, X. M.; LaRue, J.; Cooper, R.; Wodtke, A. M.; Wang, Z.; Li, Z. Y.; Wang, B.; Yang, J. L.; Hou, J. G. *Chem. Sci.* **2010**, *1*, 575.
(36) Wang, L.-Q.; Ferris, K. F.; Winokur, J. P.; Shultz, A. N.; Baer, D. R.; Engelhard, M. H. *J. Vac. Sci. Technol., A* **1998**, *16*, 3034.
(37) Onda, K.; Li, B.; Zhao, J.; Jordan, K. D.; Yang, J.; Petek, H. *Science* **2005**, *308*, 1154.
(38) Petek, H.; zhao, J. *Chem. Rev.* **2010**, *110*, 7082.
(39) Onda, K.; Li, B.; Zhao, J.; Petek, H. *Surf. Sci.* **2005**, *593*, 32.
(40) Zhao, J.; Li, B.; Onda, K.; Feng, M.; Petek, H. *Chem. Rev.* **2006**, *106*, 4402.
(41) Argondizzo, A.; Cui, X. F.; Wang, C.; Sun, H. J.; Shang, H. H.; Zhao, J.; Petek, H. *Phys. Rev. B: Condens. Matter Mater. Phys.* **2015**, *91*, 155429.
(42) Argondizzo, A.; Tan, S.; Petek, H. *J. Phys. Chem. C* **2016**, *120*, 12959.
(43) Shen, M.; Henderson, M. A. *J. Phys. Chem. Lett.* **2011**, *2*, 2707.
(44) Phillips, K. R.; Jensen, S. C.; Baron, M.; Li, S.-C.; Friend, C. M. *J. Am. Chem. Soc.* **2013**, *135*, 574.
(45) Kolesov, G.; Vinichenko, D.; Tritsaris, G. A.; Friend, C. M.; Kaxiras, E. *J. Phys. Chem. Lett.* **2015**, *6*, 1624.
(46) Guo, Q.; Xu, C. B.; Ren, Z. F.; Yang, W. S.; Ma, Z. B.; Dai, D. X.; Fan, H. J.; Minton, T. K.; Yang, X. M. *J. Am. Chem. Soc.* **2012**, *134*, 13366.
(47) Zhao, J.; Yang, J.; Petek, H. *Phys. Rev. B: Condens. Matter Mater. Phys.* **2009**, *80*, 235416.
(48) Migani, A.; Mowbray, D. J.; Iacomino, A.; Zhao, J.; Petek, H.; Rubio, A. *J. Am. Chem. Soc.* **2013**, *135*, 11429.
(49) Migani, A.; Mowbray, D. J.; Zhao, J.; Petek, H.; Rubio, A. *J. Chem. Theory Comput.* **2014**, *10*, 2103.
(50) Kresse, G.; Hafner, J. *Phys. Rev. B: Condens. Matter Mater. Phys.* **1993**, *47*, 558.
(51) Kresse, G.; Hafner, J. *Phys. Rev. B: Condens. Matter Mater. Phys.* **1993**, *48*, 13115.
(52) Kresse, G.; Hafner, J. *Phys. Rev. B: Condens. Matter Mater. Phys.* **1994**, *49*, 14251.
(53) Gundlach, L.; Ernstorfer, R.; Willig, F. *Prog. Surf. Sci.* **2007**, *82*, 355.
(54) Kresse, G.; Joubert, D. *Phys. Rev. B: Condens. Matter Mater. Phys.* **1999**, *59*, 1758.
(55) Perdew, J. P.; Burke, K.; Ernzerhof, M. *Phys. Rev. Lett.* **1996**, *77*, 3865.
(56) Kowalski, P. M.; Meyer, B.; Marx, D. *Phys. Rev. B: Condens. Matter Mater. Phys.* **2009**, *79*, 115410.
(57) Craig, C. F.; Duncan, W. R.; Prezhdo, O. V. *Phys. Rev. Lett.* **2005**, *95*, 163001.
(58) Akimov, A. V.; Prezhdo, O. V. *J. Chem. Theory Comput.* **2013**, *9*, 4959.
(59) Wang, L. J.; Long, R.; Prezhdo, O. V. *Annu. Rev. Phys. Chem.* **2015**, *66*, 549.
(60) Akimov, A. V.; Neukirch, A. J.; Prezhdo, O. V. *Chem. Rev.* **2013**, *113*, 4496.
(61) Fischer, S. A.; Duncan, W. R.; Prezhdo, O. V. *J. Am. Chem. Soc.* **2009**, *131*, 15483.
(62) Prezhdo, O. V.; Duncan, W. R.; Prezhdo, V. V. *Prog. Surf. Sci.* **2009**, *84*, 30.
(63) Nie, Z.; Long, R.; Sun, L.; Huang, C.-C.; Zhang, J.; Xiong, Q.; Hewak, D. W.; Shen, Z.; Prezhdo, O. V.; Loh, Z.-H. *ACS Nano* **2014**, *8*, 10931.
(64) Duncan, W. R.; Prezhdo, O. V. *Annu. Rev. Phys. Chem.* **2007**, *58*, 143.

DOI: 10.1021/jacs.6b08725
J. Am. Chem. Soc. 2016, 138, 13740−13749

(65) Migani, A.; Mowbray, D. J.; Zhao, J.; Petek, H.; Rubio, A. *J. Chem. Theory Comput.* **2014**, *10*, 2103.
(66) Migani, A.; Mowbray, D. J.; Iacomino, A.; Zhao, J.; Petek, H.; Rubio, A. *J. Am. Chem. Soc.* **2013**, *135*, 11429.
(67) Reeves, K. G.; Schleife, A.; Correa, A. A.; Kanai, Y. *Nano Lett.* **2015**, *15*, 6429.
(68) Sun, H.; Mowbray, D. J.; Migani, A.; Zhao, J.; Petek, H.; Rubio, A. *ACS Catal.* **2015**, *5*, 4242.
(69) Ji, Y. F.; Wang, B.; Luo, Y. *J. Phys. Chem. C* **2014**, *118*, 21457.
(70) Cheng, H.; Selloni, A. *Langmuir* **2010**, *26*, 11518.
(71) Abuabara, S. G.; Rego, L. G. C.; Batista, V. S. *J. Am. Chem. Soc.* **2005**, *127*, 18234.
(72) Monti, A.; Negre, C. F. A.; Batista, V. S.; Rego, L. G. C.; de Groot, H. J. M.; Buda, F. *J. Phys. Chem. Lett.* **2015**, *6*, 2393.
(73) Torres, A.; Oliboni, R. S.; Rego, L. G. C. *J. Phys. Chem. Lett.* **2015**, *6*, 4927.
(74) Zhukov, V. P.; Tyuterev, V. G.; Chulkov, E. V.; Echenique, P. M. *Int. J. Photoenergy* **2014**, *2014*, 738921.
(75) Morishita, T.; Hibara, A.; Sawada, T.; Tsuyumoto, I. *J. Phys. Chem. B* **1999**, *103*, 5984.
(76) Deinert, J. C.; Wegkamp, D.; Meyer, M.; Richter, C.; Wolf, M.; Stähler, J. *Phys. Rev. Lett.* **2014**, *113*, 057602.

DOI: 10.1021/jacs.6b08725
J. Am. Chem. Soc. 2016, 138, 13740−13749